order to stabilize the system energy, V_2 has to decrease by ΔV_2 to move to the hatching region. Therefore, the energy of the system will be stabilized by the decrease of V_2 even if V_1 increases. This is the underlying mechanism in the dynamic hydrogen bonding which was elucidated in section IIA. Indeed, in Figure 4, we have shown the vibronic attraction using the change of the binding potential energy as R decreases from 2.729 to 2.660 Å. Consequently, the contraction of lattice spacing suggested by Anderson and Lippincott will be explained by this vibronic effect.[8]

C. Isotope Effects. In this subsection, the isotope effects are explained. Apparently, the isotope effect of the dynamic potential energy E is solely due to e. In Figure 11, we shall show the e which has been obtained as the eigenvalue of eq 12 for each case H^+ and D^+. It should be noted that the derivative de/dR corresponds to the vibronic attractive force for the N–N bond. There are two regions: (I) $R > 2.65$ Å, where the attractive force of H^+ is greater than that of D^+, and (II) $R < 2.65$ Å, where the attractive force of D^+ is greater than that of H^+. The origin of the clear separation into I and II may be explained as follows.

Using the analytical parameters of the potential, the force may be decomposed into two terms:

$$\frac{de}{dR} = \frac{\partial e}{\partial V_1}\frac{dV_1}{dR} + \frac{\partial e}{\partial V_2}\frac{dV_2}{dR} \tag{16}$$

Now, in the region I, the H^+ is bound little with respect to the top of the barrier (see Figure 7a). In this region, the vibronic force de/dR given by eq 16 may be approximated as

$$\frac{de}{dR} \sim \frac{\partial e}{\partial V_2}\frac{dV_2}{dR} \tag{17}$$

because we find from Figure 4 that the relation $|dV_1/dR| \ll |dV_2/dR|$ holds in $R = 2.729$ Å. On the other hand, from Figure 9, we have the following relationship:

$$\left|\frac{\partial e}{\partial V_2}(H^+)\right| > \left|\frac{\partial e}{\partial V_2}(D^+)\right| \tag{18}$$

Combining eq 18 with eq 17, one can see directly that the attractive vibronic force is stronger for H^+ than for D^+ in region I, because dV_2/dR is considered the same for both H^+ and D^+.

Next, in region II where R is less than 2.65 Å, the H^+ is not tightly bound. In this region, the first term of the vibronic force de/dR, which was omitted in eq 17, should play and important role because we known $|dV_1/dR| \geq |dV_2/dR|$ in Figure 4. On the other hand, from Figure 9, we have the following relationship:

$$\left|\frac{\partial e}{\partial V_1}(H^+)\right| < \left|\frac{\partial e}{\partial V_1}(D^+)\right| \tag{19}$$

The combination of eq 19 with eq 16 leads to the result that a more drastic weakening of the attractive force of H^+ occurs as compared with that of D^+ in the region II. In the region, a contraction of the lattice spacing may be brought about when D^+ is substituted for H^+. This can be called the inverse isotope effect and might be connected to the experimental results[3] that were mentioned in the Introduction.

III. Concluding Remarks

In the present paper, we have studied the mechanism of the dynamic hydrogen bonding induced by the zero-point vibration of proton. A large isotope effect has been observed for the lattice-binding force. The criterion of the "attraction" of the lattice-binding force has been given. In our model system, the "lattice" distance R is contracted from the "static" equilibrium distance $R_{eq} = 2.729$ Å to the dynamic equilibrium distance 2.660 Å by the vibronic effect, and this effect is larger in H^+ than in D^+. The theoretical origin has been clarified by the distinct relationship between the barrier height in proton tunneling and the binding potential of the lattice as a function of the lattice distance. Moreover, the inverse isotope effect has been predicted in a range of rather small lattice spacings and may be applicable to explanation for the experimental results.[3,7] In this relation, it is worthwhile mentioning that X-ray analysis, or the more powerful neutron diffraction analysis, cannot distinguish the following two cases: (a) the case in which the proton oscillates in a symmetric single-minimum potential at the middle point, and (b) the case in which it is distributed at random in a symmetric double-minimum potential.[3] Therefore, more accurate experimental work is recommended in order to validate the present theory.

Because the problem treated in this paper is universal for general proton dynamics,[11] further application for the corresponding fields should be enhanced in future.

Acknowledgment. This work was supported by a Grant-in-Aid for Scientific Research from the Ministry of Education of Japan, for which the authors express their gratitude. We are also grateful to the Computer Center of the Institute for Molecular Science and Data Processing Center for Kyoto University for their generous permission to use the HITAC M-680H and S-810, and the FACOM M-780 and VP-200 computers, respectively.

Stirring in Chemical Reactions

Panos Argyrakis[†,‡] and Raoul Kopelman*[,‡]

Department of Physics 313-1, University of Thessaloniki, GR-54006 Thessaloniki, Greece, and Department of Chemistry, University of Michigan, Ann Arbor, Michigan 48109-1055 *(Received: February 22, 1988; In Final Form: June 8, 1988)*

Monte Carlo simulations of diffusion- and/or convection-controlled homoreactant (A + A) and heteroreactant (A + B) binary kinetics are given for one-, two-, and three-dimensional lattices and for disordered fractal lattices (percolation clusters in two and three dimensions). The rate laws are compared for different degrees and methods of convective stirring, including global versus local stirring in space and continuous versus periodic stirring in time. The results are parametrized in terms of the fractional time exponent of the reciprocal reactant density.

Introduction

To stir well is the universal instruction for chemical reactions. However, efficient convective stirring is not always possible. This is especially true for heterogeneous reactions, surface reactions, solid-state reactions, and reactions in viscous and/or restricted domains. It is difficult to stir such reactions. Thus, the distinction between well-stirred and self-stirred reactions is of both theoretical and practical interest. In addition, most solid-state "physical" reactions, e.g., electron–hole recombination or exciton–exciton

[†] University of Thessaloniki.
[‡] University of Michigan.

0022-3654/89/2093-0225$01.50/0

annihilation, are self-stirred, diffusion-limited reactions. Also, many biological and biophysical reactions, such as fluorescence quenching, are mostly in the self-stirred regime. Here we give characteristic examples for two extreme cases of "diffusion-limited" reactions, the constantly and totally stirred reaction and the totally unstirred reaction, as well as for various cases of intermediate stirring. The unstirred reactions are still "self-stirred" via diffusion. It has been shown[1] that diffusive (self-) stirring is quite efficient in homogeneous, three-dimensional space. However, for low-dimensional and/or heterogeneous media, self-stirring is inefficient. We concentrate thus on low-dimensional and "fractal" spaces, where self-stirring is synonymous with "understirring".

The traditional formalism for homogeneous reactions[2] expresses the rate constant K in terms of the cylindrical volume V swept out by the reacting molecules (cross section a times mean distance l) per unit time:

$$K = \mathrm{d}V/\mathrm{d}t \qquad \mathrm{d}V = a\,\mathrm{d}l \tag{1a}$$

$$K = a\,\mathrm{d}l/\mathrm{d}t \tag{1b}$$

For diffusion-limited reaction kinetics the equivalent Smoluchowski approach[2,3] replaces the mean velocity $\mathrm{d}l/\mathrm{d}t$ by the diffusion constant (D), for long times

$$K = a'D \qquad t \to \infty \quad (a' = \text{constant}) \tag{2}$$

In a microscopic model where the Brownian motion is described in terms of molecular random walk,[4-6] $\mathrm{d}V/\mathrm{d}t$ is naturally substituted by the volume which the walker sweeps out in unit time:

$$K = b\,\mathrm{d}n/\mathrm{d}t \tag{3}$$

where b is the "volume" of the walker and $\mathrm{d}n/\mathrm{d}t$ is the number of such volumes swept out in unit time. For instance, on a cubic lattice, with unit cell volume b, the walker sweeps out $\mathrm{d}n$ unit cells per unit time $\mathrm{d}t$. The question arises, How does one count $\mathrm{d}n$? Is it (I) the total number of unit cells swept out by the walker, or is it (II) the *distinct* number of such cells swept out, on the average? While for a well-stirred system (convection-stirred) the first approach (I) is correct, for a system that is only "self-stirred" by molecular diffusion, the second approach (II) applies.[1] In a three-dimensional, isotropic system (like a cube) the difference between (I) and (II) is less than a factor of 2 (1.5164 for long times).[4] However, for lower dimensional systems the difference becomes dramatic (many orders of magnitude) and, moreover, K becomes a function of time (even at $t \to \infty$) in case II. Thus, the problem is of much interest to heterogeneous reactions (e.g., surface reactions), where convection stirring (on the surface or inside the pores) is not a likely process.

We give here simulations of the rate constant for the reaction

$$\mathrm{A} + \mathrm{A} \to 0 \tag{4}$$

as well as

$$\mathrm{A} + \mathrm{B} \to 0 \tag{5}$$

where the reaction product is either a photon (exciton annihilation reaction) or a species that leaves the active surface (as $\mathrm{A}_2\uparrow$ or $\mathrm{AB}\uparrow$). The simulations are performed for cubic lattices, square lattices, two- and three-dimensional critical percolation clusters, and a one-dimensional lattice. We demonstrate the effects of various modes and degrees of stirring via the conventional time evolution of the macroscopic (global) reactant densities and the related, fractal, time exponents. In a forthcoming publication we will present the microscopic (local) picture in terms of nearest-neighbor distribution functions.

Method of Calculations

All computer simulations are performed using well-known Monte Carlo methods. First, lattices are generated as follows: for the case of a perfect lattice all sites are identical; for percolating clusters binary lattices are generated, the cluster distribution is performed, the largest percolating cluster is isolated, and all other clusters are erased. The binary concentration is chosen as p_c = 0.595 (2-D), and p_c = 0.315 (3-D). Typical sizes are 10000 sites (1-D), 200 × 200 (2-D), and 40 × 40 × 40 (3-D). A certain initial particle population is placed at random on the lattice, with only one particle allowed to occupy a lattice site; typically, the initial particle density ρ_0 is 0.05 particle/site, for each species present. In the case of the A + A reaction the particles carry no label, while in the case of the A + B reaction each particle at time t = 0 is labeled either A or B. The diffusional motion is simulated by allowing each particle to perform a random walk with steps leading to its nearest-neighbor sites only. If during this walk a particle comes to a site that is occupied by another particle in the case of the A + A reaction, the two particles react, A_2 is generated, and the 2A particles are annihilated. In the case of the A + B reaction the same thing happens if the encounter is between an A and a B particle, while nothing happens if two A or two B particles collide. In this event, while there is no reaction between the two like particles, the particle that attempted to move returns to its original position and consumes one time step altogether. Similarly, the generated AB species leaves the system.

In the diffusion-limited case, after the reaction starts, the particle density is monitored as a function of time without any interference in the reaction process. In the well-stirred case after each time step all remaining particles rerandomize their positions. This is done by simply removing all particles and repositioning them randomly on the lattice without any memory of their previous positions. Similarly, the particle density is monitored as a function of time.

We have devised three models for the intermediate cases between the diffusion-limited and the fully stirred ones. (I) Periodic stirring: Stirring occurs periodically in time only; i.e., all particles are stirred once every several hundred steps, typically here once every 400 steps. (II) Partial stirring: Stirring occurs constantly but only for a certain percentage m of the remaining particles (randomly chosen). The fraction m is an adjustable parameter which is varied in these calculations between m = 0.01 and m = 0.1. (III) Local stirring: In this mode all particles are constantly stirred (i.e., repositioned on a different site), but each particle is allowed to relocate only $\pm n$ sites away in each direction. This is done by retaining memory of its previous position. Again, n is an adjustable parameter which is varied here between n = 1 and n = 200 (1-D) and n = 1 and n = 5 (2-D and 3-D).

For each case usually 500 realizations are performed and the results are averaged over these.

Results and Discussion

The classical rate equation for the reaction A + A → 0 is obviously

$$-\mathrm{d}\rho/\mathrm{d}t = K\rho^2 \tag{6}$$

and the integrated rate equation is

$$\rho^{-1} - \rho_0^{-1} = Kt \tag{7}$$

where K is a constant, ρ is the reactant density at time t, and ρ_0 that at t = 0.

The above implies efficient stirring. For self-stirred reactions it has been shown in recent years that K in eq 6 generally becomes time dependent even for long times[4,5] and that eq 7 takes the form

$$\rho^{-1} - \rho_0^{-1} = k_0 t^{-f} \tag{8}$$

where f is a fractional exponent, $0 < f < 1$. For instance, for the reaction of eq 4

$$f = d_s/2 \qquad d_s < 2 \tag{9}$$

where d_s is the spectral (fraction) dimension.[5] For $d_s > 2$, f =

(1) Argyrakis, P.; Kopelman, R. *J. Phys. Chem.* **1987**, *91*, 2699.
(2) Atkins, P. W. *Physical Chemistry*; Freeman: New York, 1985. Noyes, R. M. In *Progress in Reaction Kinetics*; Porter, G., Ed.; Pergamon: New York, 1961; Vol. 1, p 128. Keizer, J. *Acc. Chem. Res.* **1985**, *18*, 235.
(3) Smoluchowski, M. V. *Phys. Z.* **1916**, *17*, 585.
(4) Kopelman, R.; Argyrakis, P. *J. Chem. Phys.* **1980**, *72*, 3053.
(5) Kopelman, R. *J. Stat. Phys.* **1986**, *42*, 185.
(6) Argyrakis, P.; Kopelman, R. In *Advances in Chemical Reaction Kinetics*; Rentzepis, P. M., Capellos, C., Eds.; Dordrecht: Holland, 1986; p 339.
(7) Kopelman, R.; Hoshen, J.; Newhouse, J. S.; Argyrakis, P. *J. Stat. Phys.* **1983**, *30*, 355.

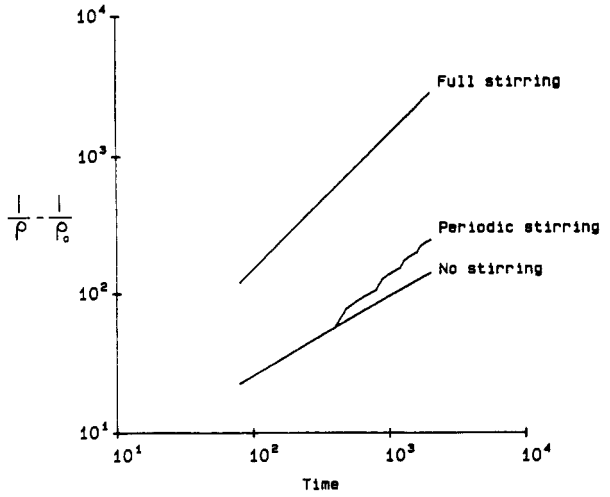

Figure 1. Density plot for the A + A reaction as a function of time. Here $1/\rho - 1/\rho_0$ is plotted vs t for the 1-D reactions. The diffusion-limited, fully stirred, and the periodically stirred (once in 400 steps) reactions are shown.

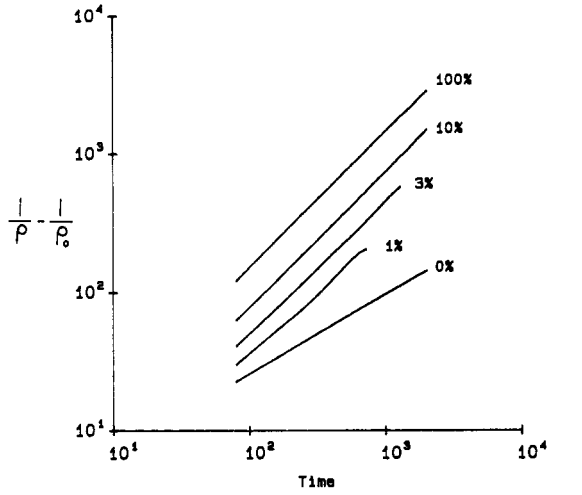

Figure 2. Density plot (similar to Figure 1) for 1-D A + A reactions with partial stirring. Here m = 0, 0.01, 0.03, 0.1, and 1.0.

1; $d_s = 2$ is a marginal dimension. For the reaction of eq 5 it has been claimed[8-11] that

$$f = d_s/4 \qquad d_s < 4 \tag{10}$$

For $d_s > 4$, $f = 1$ again, and $d_s = 4$ is a marginal dimension. Equations 9 and 10 imply random initial conditions for the A and B reactants. If, however, A and B are produced pairwise, e.g., AB → A + B, eq 9 applies[12] rather than eq 10.

Figures 1–9 give the trends for the global density dependence as a function of time.

Figure 1 shows a plot of $1/\rho - 1/\rho_0$ for a 1-D reaction. The diffusion-limited curve is not absolutely straight, since there is a difference between the short-time and long-time limits.[8-11] The short-time limit gives a slope (see eq 8) $f = 0.57$, while the long time gives $f = 0.51$. The fully stirred case gives a slope that is very close to 1.00 ($f = 0.98$) for the whole range. The periodically stirred case shows a wavy curve with a sudden rise occurring at every point of stirring. The trends are rather clear: when all remaining particles are stirred, this has an effect of breaking up the spatial and temporal correlations in particle positions that have been built up during the course of the reaction. If this stirring is constant, no such correlations are built up, and, therefore, the classical result ($f = 1$) is expected. When periodic stirring takes place, the correlations are built up to the point of stirring, at which time stirring causes their breakup. This order of events is then repeated.

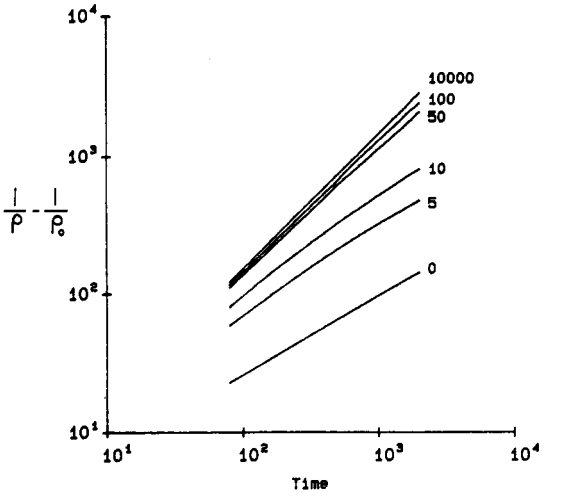

Figure 3. Density plot for 1-D A + A reactions with local stirring. Here n = 0, ±5, ±10, ±50, ±100, and ±10 000.

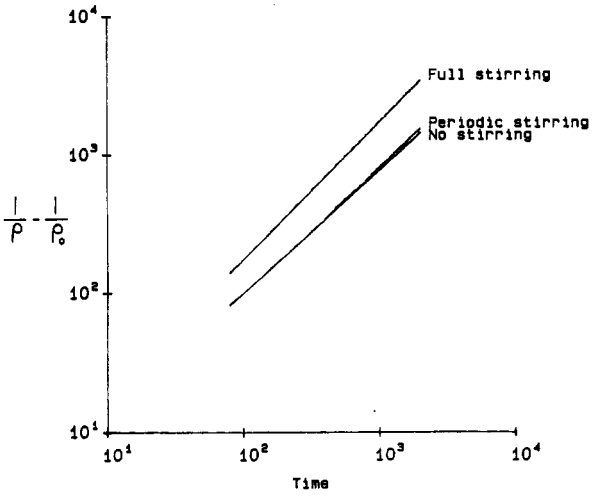

Figure 4. Density plot for 2-D A + A reactions, similar to Figure 1.

Figure 2 shows the effects of partial stirring on the 1-D reaction (model II). A crossover effect is seen here: the exponent f changes from $f = 0.5$ (no stirring) to $f = 0.65$ ($m = 0.01$), $f = 0.89$ ($m = 0.03$), $f = 0.98$ ($m = 0.05$, not shown), and $f = 0.98$ ($m = 0.1$ and 1.0). The curves in Figure 2 are shown progressively for shorter times, since for small values of m (e.g., $m = 0.01$) no particles are stirred when their total number falls below $m^{-1}/2$.

Figure 3 shows the effects of local stirring (model III) on the 1-D reaction. Again we observe a crossover behavior here as n increases. The exponent f changes from $f = 0.5$ (no stirring) to $f = 0.63$ ($n = \pm 5$), $f = 0.69$ ($n = \pm 10$), $f = 0.90$ ($n = \pm 50$), $f = 0.97$ ($n = \pm 100$), and $f = 0.98$ ($n = \pm 10\,000$, i.e., the whole lattice).

Figure 4 shows the results for a 2-D reaction. The same trends hold here as previously. Here, for the unstirred case, $f = 0.84$ for the short-time limit and $f = 0.94$ for the long-time limit. The well-stirred case has $f = 0.99$, while the periodically stirred case shows the same wavy curve but with much smaller fluctuations than in the 1-D case (Figure 1). This is expected since the difference in the f values is much smaller now: f ranges from 0.50 to 0.98 in one dimension but from 0.90 to 0.99 in two dimensions.

Figures showing the effects of partial and local stirring for the 2-D reactions are given in the supplementary material. (See paragraph at end of paper regarding supplementary material.) We note here that it takes a much smaller n ($n = \pm 5$) to reach the classical behavior in 2-D than in 1-D, where one needs $n = \pm 200$. This is, of course, due to the different nature of the two dimensionalities (in 1-D $n = \pm 5$ means 10 sites but 100 sites in 2-D).

(8) Ovchinnikov, A. A.; Zeldovich, Y. B. *Chem. Phys.* **1978**, *28*, 215.
(9) Toussaint, D.; Wilczek, F. *J. Chem. Phys.* **1983**, *78*, 2642.
(10) Kang, K.; Redner, S. *Phys. Rev. Lett.* **1984**, *52*, 955.
(11) Ben-Avraham, D. *J. Chem. Phys.* **1988**, *88*, 941.
(12) Li, L.; Kopelman, R. *J. Lumin.* **1988**, *40–41*, 688.

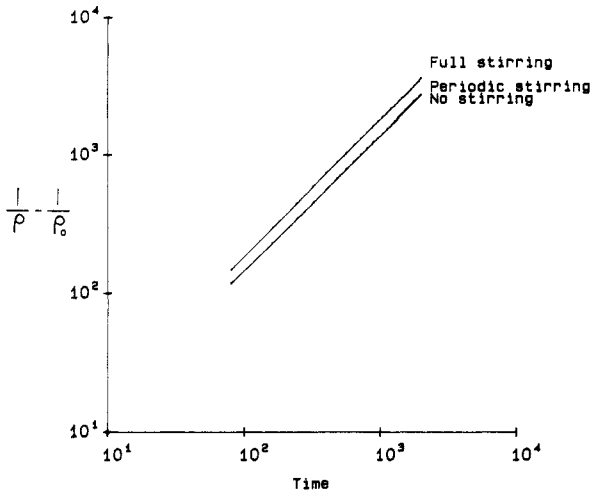

Figure 5. Density plot for 3-D A + A reactions (similar to Figures 1 and 4).

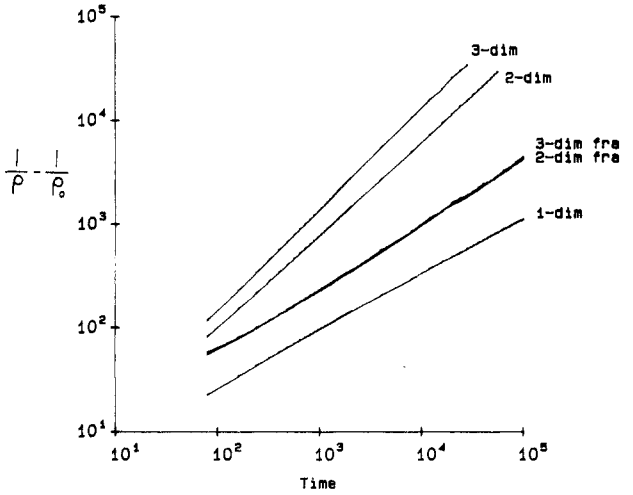

Figure 6. Diffusion-limited behavior for the A + A reactions as a function of dimensionality, for 1-D, 2-D, 3-D perfect lattices and 2-D, 3-D fractal lattices (percolating clusters). For the fractal lattices (maxiclusters) the myopic ant model has been used. The associated exponents are given in Table I.

TABLE I: f Values for the A + A Diffusion-Limited Reaction

lattice	f (short time)	f (long time)
1-D	0.57	0.51
2-D fractal	0.59	0.63
3-D fractal	0.57	0.63
2-D	0.84	0.94
3-D	0.98	0.98

Figure 5 gives the results for 3-D reactions. The diffusion-limited case has $f = 0.98$, while the well-stirred case has $f = 0.99$. There are hardly any consequences due to periodic stirring, as we see from the corresponding curve in this figure. Also, when the effects of partial stirring and local stirring were studied, we found that all values were bounded by the results $f = 0.98$ and 0.99.

Figure 6 gives a summary for the 1-D, 2-D, and 3-D diffusion-limited cases, together with the results for the fractal lattices. The latter are binary lattices (in 2-D and 3-D) at the critical percolation threshold (maxicluster only). Table I gives a summary of the reaction exponents for these processes. As expected, the f values for the reactions on fractal lattices approach the well-known value of $f = {}^2/_3$, for both 2-D and 3-D. This is a manifestation[5] of the result that the random walk property S_n behaves the same in both dimensionalities in the fractal lattices, a truly unique observation in critical phenomena.

Figure 7 is similar to Figure 1 but for the A + B reaction. The diffusion-limited f varies here from $f = 0.40$ (short time) to $f =$ 0.32 (long time). The fully stirred case shows a totally classical result, $f = 1.01$. The periodically stirred case shows the wavy curve of the A + A reaction. However, here we observe that this effect is more pronounced, due to the inherent segregation[8-10] that takes place in the A + B reaction, but is absent in the A + A reaction. Figure 8 and figures in the supplementary material show for the A + B reaction the cases seen for the A + A reactions in Figures 2–6 (and in the supplementary material). Some quantitative values are given in Table II. We note that in Figure 8 the 2- and 3-D percolation cluster curves do not overlap, in contrast to the A + A case (Figure 6). Qualitatively, however, the A + B behavior follows the A + A behavior. Quantitatively, the effect of stirring is more pronounced in the A + B case. Due to the segregation of A and B particles in the diffusion-limited case,[8-15] the f values

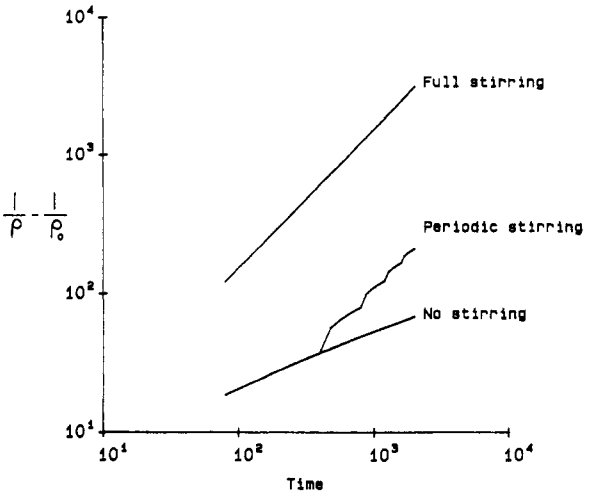

Figure 7. Density plot for 1-D A + B reactions, plotted in a similar fashion as the A + A reactions (Figure 1).

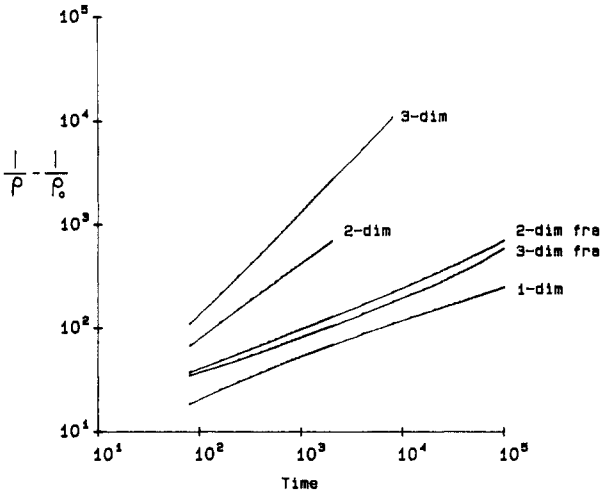

Figure 8. Diffusion-limited behavior for the A + B reactions as a function of dimensionality, for 1-D, 2-D, 3-D perfect lattices and 2-D, 3-D fractal lattices (percolating clusters). For the fractal lattices (maxiclusters) the blind ant model has been used. The associated exponents are given in Table II.

TABLE II: f Values for the A + B Diffusion-Limited Reaction

lattice	f (short time)	f (long time)
1-D	0.40	0.32
2-D fractal	0.39	0.45
3-D fractal	0.35	0.45
2-D	0.72	
3-D	1.00	

(13) de Gennes, P. G. *C. R. Seances Acad. Sci., Ser. 2* **1983**, *296*, 881.
(14) Torney, D. C.; McConnell, H. W. *Proc. R. Soc. London, A* **1983**, *387*, 147.
(15) Anacker, L. W.; Kopelman, R. *Phys. Rev. Lett.* **1987**, *58*, 289.

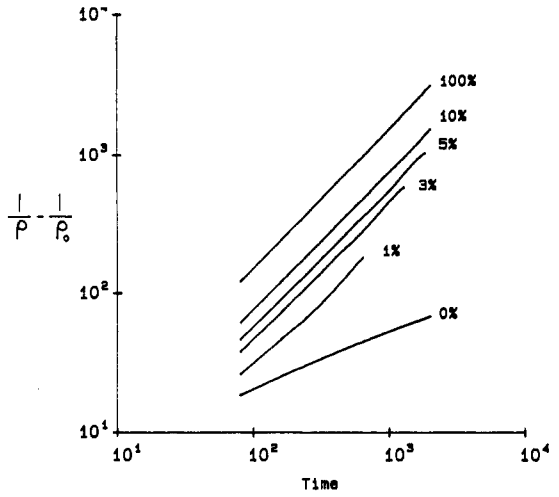

Figure 9. Density plot (similar to Figure 2) for 1-D A + B reactions with partial stirring. Here m = 0, 0.01, 0.03, 0.05, 0.1, and 1.0.

go to lower values at long times (compare eq 8 and 9). This leaves a larger numerical gap between the self-stirred and well-stirred cases even at intermediate times (compare Tables I and II), to be bridged by incomplete stirring (whether periodic, partial, or local), except in three dimensions. We note that the A–B segregation effect is more sluggish the higher the dimension. Thus, our simulations do not reach the asymptotic values of eq 9. Even literature simulations with much longer reaction times[9-12] have not quite reached these values, especially for the higher dimensions (2 and 3). Regarding the crossover times and crossover behaviors of the diffusion-limited reactions, our data resemble previous studies.[9-11] Obviously, for $d < 3$, eq 8 is only valid at $t \rightarrow \infty$; exact results for one and two dimensions have been given by Torney and McConnell[14,16] and others.[17] The deviations from eq 8 manifest themselves as a time dependence of f. [The time dependence of f for $d = 1$ follows that exact solution;[16] for $d > 1$ it is not so obvious.] Our interest here is focused on the effects of mixing. As complete stirring gives the classical result, it obviously erases all crossover phenomena (Figures 1–5, 7, and 9). However, even a small degree of stirring can have drastic effects on the crossover phenomena. (See the inversion of curvature for 1% stirring in Figure 9.)

Complete stirring assures random (Poissonian, Hertzian[18,19]) distributions of reactants. Incomplete or no stirring, at low dimensions, gives rise to nonrandom (partially ordered) kinetic distributions.[8-11,15,20] Such distributions have been derived and will be given in a subsequent paper, together with a more complete interpretation of the kinetic data.

Our overall conclusion is that "a little stirring goes a long way". In addition, the nature of the stirring is important. We have demonstrated the effects of global versus local stirring and continuous versus periodic stirring. The dimensionality of the medium is quite important; in low dimensions the effects of understirring are drastic. Finally, for heteroreactant (A + B) kinetics, understirring leads to reactant segregation in low dimensions.

Acknowledgment. This work was supported by NSF Grant DMR-8303919 and by the donors of the Petroleum Research Fund, administered by the American Chemical Society.

Supplementary Material Available: Figures S1–S7 representing additional cases of A + A and A + B reactions (7 pages). Ordering information is given on any current masthead page.

(16) Torney, D. C.; McConnell, H. M. *J. Phys. Chem.* **1983**, *87*, 1441.
(17) Spouge, J. L. *Phys. Rev. Lett.* **1988**, *60*, 871, 1885.
(18) Hertz, P. *Math. Ann.* **1909**, *67*, 387.
(19) Chandrasekhar, S. *Rev. Mod. Phys.* **1943**, *15*, 1.
(20) Kopelman, R. *Science* **1988**, *241*, 1620.

Vibrational to Electronic Energy Transfer from HF(v=2,3) to NF($a^1\Delta$)

J. Habdas† and D. W. Setser*

Department of Chemistry, Kansas State University, Manhattan, Kansas 66506 *(Received: June 28, 1988; In Final Form: October 5, 1988)*

The excitation of NF($b^1\Sigma^+$) by the energy-transfer reaction between HF(v=2,3) and NF($a^1\Delta$) has been observed in a flow reactor at room temperature. The HF(v=2,3) molecules were generated by reaction of F atoms with a fuel, and NF($a^1\Delta$) was generated by the reaction of excess F atoms with HN_3. By simultaneous observation of the HF(v=2,3), NF($a^1\Delta$), and NF($b^1\Sigma^+$) concentrations via their emission intensities, a rate constant of (0.5–1.5) × 10^{-12} cm^3 molecule^{-1} s^{-1} was established for the vibrational-to-electronic energy-transfer reaction. This value is in general accord with the rate constant deduced from the reverse step, the quenching of NF(b) by HF(v=0) at 300 K.

Introduction

In 1970 Clyne and White[1] observed chemiluminescence from the NF($b^1\Sigma^+$–$X^1\Sigma^+$) and NF($a^1\Delta$–$X^1\Sigma^+$) transition from the reactions of NF_2 with H, N, and O atoms. They suggested that NF(b) was produced by electronic energy transfer from some energetic species generated from NF_2 radicals. Herbelin and Cohen[2] reexamined the H/NF_2 system and concluded that energy transfer between electronically excited HF($a^1\Delta$) and vibrationally excited HF($v\geq2$) was responsible for formulation of NF($b^1\Sigma^+$):

$$\mathrm{HF}(v{=}2) + \mathrm{NF}(a^1\Delta,v{=}0) \xrightarrow{k^{2,0}_{a,b}} \mathrm{HF}(v{=}0) + \mathrm{NF}(b^1\Sigma^+);\quad \Delta H_0^\circ = -298\ \mathrm{cm}^{-1} \quad (1a)$$

$$\mathrm{HF}(v{=}3) + \mathrm{NF}(a^1\Delta,v{=}0) \xrightarrow{k^{3,1}_{a,b}} \mathrm{HF}(v{=}1) + \mathrm{NF}(b^1\Sigma^+);\quad \Delta H_0^\circ = 41\ \mathrm{cm}^{-1} \quad (1b)$$

There is a good energy match for HF(v=2,3) with the energy defects being as shown for reactants and products in the $J = 0$ state, and reaction 1 has become the benchmark for both practical

† Present address: Department of Chemistry, Silesian University, 40006 Katowice, Szkolna 9, Poland.

(1) Clyne, M. A. A.; White, I. F. *Chem. Phys. Lett.* **1970**, *26*, 465.
(2) Herbelin, J. M.; Cohen, N. *Chem. Phys. Lett.* **1973**, *20*, 605.

0022-3654/89/2093-0229$01.50/0